Studies on Dynamics of a Unmanned Aerial Vehicle With Variable-Span and Variable-Sweep Wing

Jie Guo and Guantong Yang***

** Key Laboratory of Dynamics and Control of Flight Vehicle, Ministry of Education, Department of Aerospace Engineering, Beijing Institute of Technology, Beijing, 100081*

Abstract

In order to make the UAVs maintain optimal flight performance in a variety of flight conditions, a new concept of the variable-configuration unmanned aerial vehicle is proposed in this paper that combines two different deformation modes, which expands the morphing degree of freedom of the UAV compared with the one of single mode of deformation. Based on this morphing concept, the aerodynamic characteristics under the typical static configurations of this morphing UAV is calculated and analyzed. Then, the multi-rigid-body kinetic model of the UAV is established through designating the fuselage as the primary rigid body and the variable-span wing and variable-sweep wing as the subsidiary rigid bodies.

1. Introduction

The traditional unmanned aerial vehicle (UAV) generally only has a single flight mode, and its optimal functionality and performance of flight is often embodied in certain tasks, such as low-speed cruising or high-speed penetration. In recent years, many higher requirements, in terms of maneuverability, reliability, especially the multi-task capability, are put forward to the new generation of UAVs. The variable-configuration UAV, also called the morphing UAV, as a new concept of multi-purpose unmanned aircraft which is predicted with great application prospects in both military and civilian fields, has gained more and more attentions. Reasonable design of the variable aerodynamic configuration will enables UAVs to meet the requirements of the large airspace and speed domain, and maintain optimal flight performance in a variety of flight conditions so that the UAVs are able to perform multiple tasks beyond the capability of the conventional ones. However, the research of the large-scale deformation UAVs is still in the initial exploratory stage in both theory and application.

Currently, the development trend of morphing flight vehicle has two main directions: the integrated large-scale deformation and the local small deformation or flexible deformation based on the smart structures and smart materials[1-2]. However, the current development status of the smart material technologies can not meet the practical control requirements of the morphing flight vehicles. Therefore, most of the current studies are still stuck in the theoretical and experimental exploration stage. In contrast, the rigid large-scale deformation flight vehicle has made some representative progress in the engineering practice.

Janisa and Darryll use a standard six-degree of freedom model to describes the dynamics of an aircraft with morphing-span wing, and then analyze the differences of the dynamic behavior between the morphing-span wing and the conventional ailerons[3]. Onur Bilgen, together with his Virginia Tech Wing Morphing Design Team, has developed a completely servo-less, piezoelectric controlled, wind tunnel and flight tested, remotely piloted aircraft[4]. Kenneth and Jeffrey concern about the effect on aircraft performance brought by the morphing mechanism. The benefits of using morphing wing technology in fighter aircraft configurations is analyzed during their research through exergy analysis and large-scale optimization to the integrated mission synthesis and operation of an air-to-air fighter[5]. For shape design of morphing airfoil sections at different aspect ratio and wing sweep based on specific missions, an optimization method is employed in Howoong's studies using strain energy needed to change from one airfoil shape to another as an additional design objective along with a drag design objective[6]. The optimization of a variable-span morphing wing for a small low-speed UAV is also studied by researchers from University of Beira Interior[7], while the drag can be reduced by 20% with the variable-span wing optimized in their research in comparison with the original fixed wing. William and Joshua focus on the multilevel design optimization approaches for sizing a morphing aircraft and the most crucial six variables are summarized in their studies as the reference design variables, which are thrust-to-weight ratio, wing loading, wing thickness-to-chord ratio, wing sweep, wing taper ratio and aspect ratio[8]. A multidisciplinary design optimization tool, based on the coupled constraints of

aerodynamic and structural morphing, is adopted by the researchers from University of Beira Interior and University of Victoria for the design of a small experimental UAV to obtain a set of optimal wing shapes for minimum drag at different flight speeds[9]. The control problems of both the morphing wing as well as the entire morphing aircraft are also discussed by many researchers[10] who presents control solutions using model-based methods that provide precise, closed-loop control of the morphing wing, of which the specific one in their research is the N-MAS wing designed by NextGen Aeronautics, and simultaneously enforce prescribed closed-loop aircraft dynamics. There are also other studies on the morphing aircraft design, especially on the system modeling[11-13], the structure design[14-15], the dynamic characteristics and the control characteristics[16-19] of the morphing aircraft.
In order to make the UAVs maintain optimal flight performance in a variety of flight conditions, a new concept of the variable-configuration unmanned aerial vehicle is proposed in this paper that combines two different deformation modes, which expands the morphing degree of freedom of the UAV compared with the one of single mode of deformation. This variable-configuration UAV shows the characteristics of both the variable-span wing and variable-sweep wing, thereby providing more deformation degree of freedom to achieve the larger-scale deformation. Based on this morphing concept, the aerodynamic characteristics under the typical static configurations of this morphing UAV is calculated and analyzed. Then, the multi-rigid-body kinetic model of the UAV is established through designating the fuselage as the primary rigid body and the variable-span wing and variable-sweep wing as the subsidiary rigid bodies. At last, a decoupling method is discussed to offset the coupling term within the dynamics process of the morphing UAV.

2. System Concepts

2.1 Morphing modes

This morphing UAV combines two different deformation modes, the variable-span wing and variable-sweep wing, shown in Fig.1. A pair of variable-sweep wings is installed symmetrically on both sides of the fuselage with the function of changing sweep angle within a certain range. Another pair of wings, fixed on the variable-sweep wings, is able to stretch along the spanwise. According to the limit position of the variable-span wing and variable-sweep wing, the morphing UAV can perform under four typical static shapes, as shown in Table 1, where $\Delta\chi$ is the sweep angle of the variable-sweep wing, while Δl represents the incremental span variable-span wing.

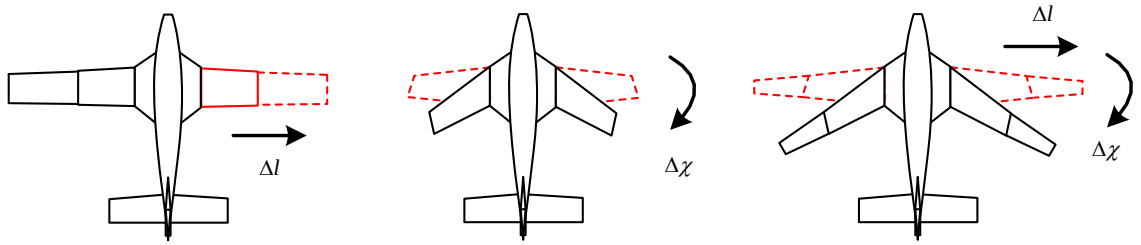

Figure 1: Morphing modes

Table 1: Geometric parameters of different shapes

	Shape features	Wing parameters
Shape 1	large sweep angle, small wingspan	$\Delta\chi = \Delta\chi_{max}, \Delta l = \Delta l_{min}$
Shape 2	large sweep angle, large wingspan	$\Delta\chi = \Delta\chi_{max}, \Delta l = \Delta l_{max}$
Shape 3	small sweep angle, small wingspan	$\Delta\chi = \Delta\chi_{min}, \Delta l = \Delta l_{min}$
Shape 4	small sweep angle, large wingspan	$\Delta\chi = \Delta\chi_{min}, \Delta l = \Delta l_{max}$

2.2 Structure and layout

Fig.2 shows two typical static shape structures of the morphing UAV under the limit positions of the morphing wings, corresponding to the shape 4 and shape 4 as defined in Table 1, and the geometric parameters are shown in Table 1. These two pairs of wings, the variable-span wing and variable-sweep wing, can functions independently so that the aerodynamic characteristics and mass distribution characteristics of the UAV can be changed along with the changes of the aerodynamic shape. This will make it possible for the UAV that the aircraft will obtain optimal aerodynamic performance under different conditions.

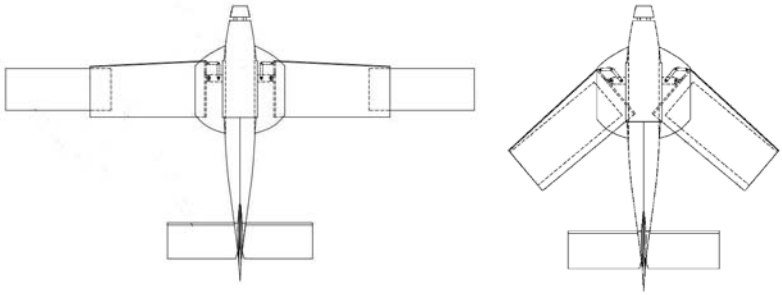

Figure 2: Structure and shapes

Table 2: Geometric parameters of different shapes

	Length L/m	Wing sweep χ /º	Wingspan l/m	Sweep of variable-sweep wing $\Delta\chi$ /º	Span of variable-span wing $\Delta l/m$
Shape 1	1.9	0	3.3	0	0.76
Shape 2	1.9	45	1.9	45	0

Furthermore, if the two variable-span wings can also operate independently, then the UAV will be in asymmetric flight status and thereby obtain additional lateral control moment. This aerodynamic effect produced by asymmetric flight can be equivalent to the role of the traditional ailerons, which can be used to achieve the attitude control of the UAV's rolling and yawing channel.

3. Aerodynamic characteristics

3.1 Aerodynamic calculation

In order to analyze the aerodynamic characteristics of the morphing UAV, the aerodynamic forces and moment of four typical shapes are calculated using empirical formula of the engineering methods under the conditions of low Mach number. The calculation state is as follows:
Mach number *Ma*: 0.06, 0.08, 0.1, 0.12, 0.14, 0.16 0.18, 0.20, 0.22, 0.24;
Angle of attack α: 0º, 2 º, 4 º, 6 º, 8 º, 10 º, 12 º, 14 º, 16 º, 18 º;
Main parameters of the aerodynamic characteristics are lift coefficient C_L, drag coefficient C_X, longitudinal static stability moment coefficient (derivative term) m_z^{α} , pitch damping moment coefficient (derivative term) $m_z^{\omega_z}$.
The main calculation result is shown in Fig.3~Fig.5.

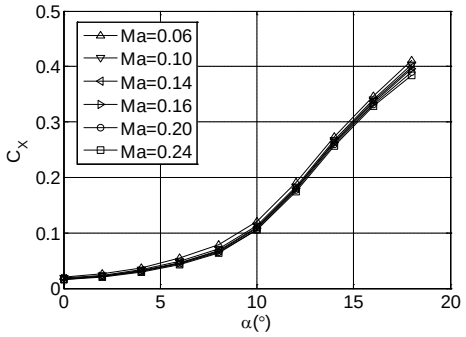

(a) Shape 1

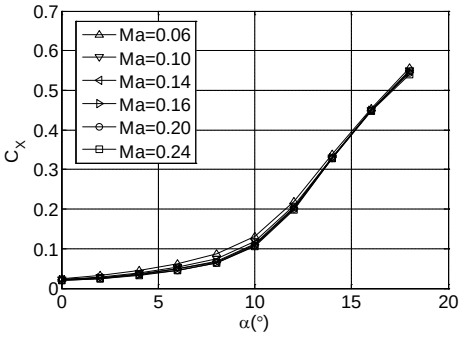

(b) Shape 2

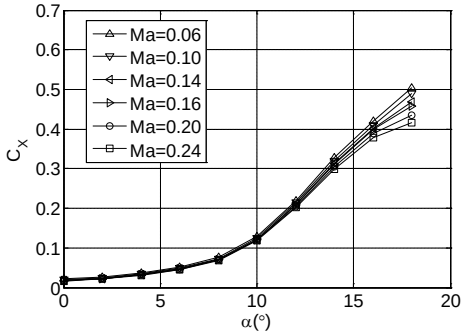

(c) Shape 3

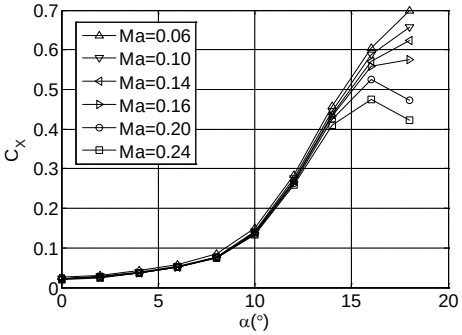

(d) Shape 4

Figure 3: Drag coefficient of four typical static shapes .

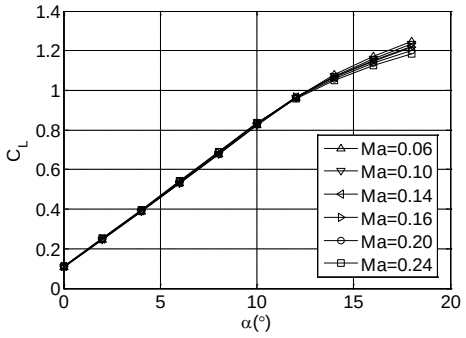

(a) Shape 1

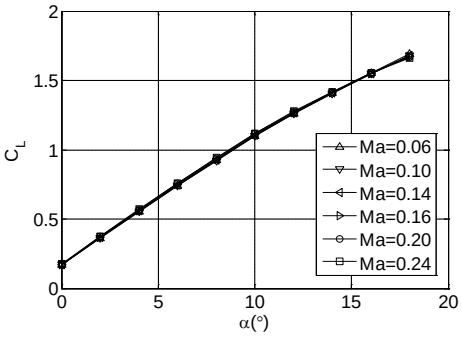

(b) Shape 2

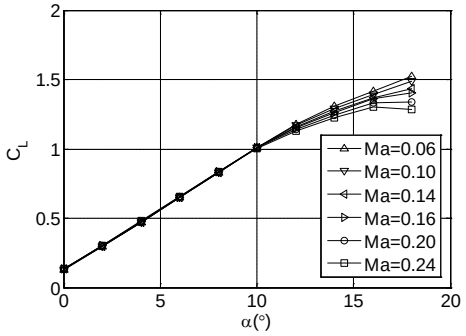

(c) Shape 3

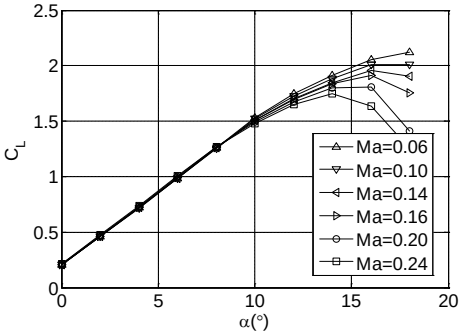

(d) Shape 4

Figure 4: Lift coefficient of four typical static shapes.

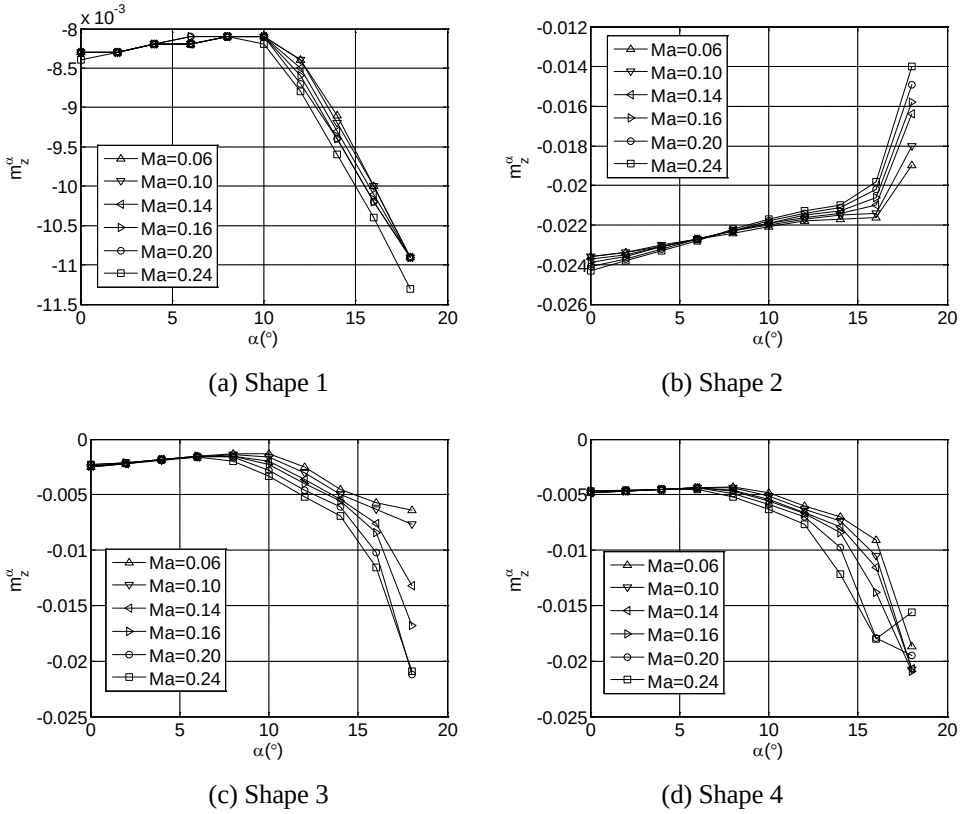

(a) Shape 1 (b) Shape 2

(c) Shape 3 (d) Shape 4

Figure 5: Longitudinal static stability moment coefficient of four typical static shapes.

3.2 Aerodynamic analysis

As shown in Fig 1~Fig 1, the aerodynamics do not show a significant change along with the Mach number *Ma* at the calculation state, while, it show almost the same change trend along with the angle of attack α except the longitudinal static stability moment coefficient and the pitch damping moment coefficient of the shape 2. It can be concluded that the main reason for this phenomenon is due to the aerodynamic characteristics of the sweep wings. As the increasing of the angle of attack, the stall phenomenon first occurs in the wingtip area of the sweep wing because of the movement trend of the boundary layer towards the wingtip. The aerodynamic pressure center will move forward when the wingtip lost lift so that the longitudinal static stability will decrease, as shown in Fig 5. Table 3 ~Table 5 give a comparison of aerodynamic characteristics under different shapes.

Table 3: Aerodynamic characteristics (*Ma*=0.2, α= 6 º)

	Lift coefficient C_L	Drag coefficient C_X	Lift-drag ratio C_L/C_X	Longitudinal static stability moment coefficient m_z^α	Pitch damping moment coefficient $m_z^{\omega_z}$
Shape 1	0.540	0.044	12.27	-0.009	-1.017
Shape 2	0.755	0.046	16.41	-0.023	-1.371
Shape 3	0.655	0.046	14.23	-0.002	-1.043
Shape 4	1.007	0.051	19.75	-0.004	-1.035

Table 4: Aerodynamic characteristics (*Ma*=0.2, α= 10 º)

	Lift coefficient C_L	Drag coefficient C_X	Lift-drag ratio C_L/C_X	Longitudinal static stability moment coefficient m_z^{α}	Pitch damping moment coefficient $m_z^{\omega_z}$
Shape 1	0.834	0.106	7.87	-0.008	-1.033
Shape 1	1.114	0.108	10.31	-0.218	-1.367
Shape 1	1.009	0.120	8.41	-0.003	-1.060
Shape 1	1.495	0.136	10.99	-0.006	-1.063

Table 5: Aerodynamic characteristics (*Ma*=0.2, α= 16 º)

	Lift coefficient C_L	Drag coefficient C_X	Lift-drag ratio C_L/C_X	Longitudinal static stability moment coefficient m_z^{α}	Pitch damping moment coefficient $m_z^{\omega_z}$
Shape 1	1.136	0.331	3.43	-0.010	-1.098
Shape 1	1.551	0.449	3.45	-0.020	-1.371
Shape 1	1.334	0.389	3.43	-0.010	-1.111
Shape 1	1.806	0.524	3.45	-0.018	-1.152

4. Mathematical modeling

4.1 Coordinate System and basic dynamic equations

To simplify the description of the morphing UAV, the fuselage coordinate system $Ox_1y_1z_1$ is introduced with coordinate origin assigned at the centroid of the fuselage. The relation of the ground coordinates system *Oxyz* and fuselage coordinate system $Ox_1y_1z_1$ is shown in Fig.6. w_i is the centroid of the *i*th wing, where the subscript *i* can be one of the four numbers 1,2,3,4, which respectively represents the lift variable-sweep wing, right variable-sweep wing, lift variable-span wing and right variable-span wing shown in Fig.7. S_i, r_{wi} and r_O are the radius vectors of the coordinate origin and the centroid of the *i*th wing.

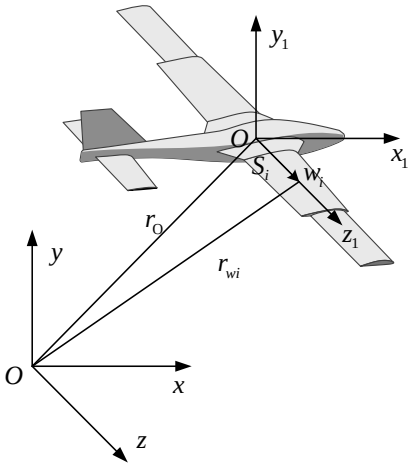

Figure 6: Coordinates system relations.

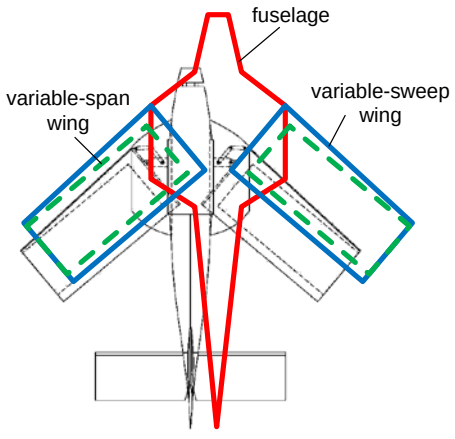

Figure 7: variable wings.

The relation between the kinematic parameters can be expressed as

$$\begin{cases} \boldsymbol{V}_o = \boldsymbol{V}_f = \dfrac{d\boldsymbol{r}_o}{dt} \\ \boldsymbol{V}_{S_i} = \dfrac{d\boldsymbol{S}_i}{dt} = \dfrac{d\boldsymbol{r}_{g_i}}{dt} - \dfrac{d\boldsymbol{r}_o}{dt} = \boldsymbol{V}_i - \boldsymbol{V}_o \end{cases} \tag{1}$$

where the subscript *f* indicates the fuselage. Generally, the aircraft is a variable mass system, of which the basic dynamic equations are given as

$$\begin{cases} m(t)\dfrac{d\boldsymbol{V}}{dt} = m(t)\left(\dfrac{\delta \boldsymbol{V}}{\delta t} + \boldsymbol{\Omega} \times \boldsymbol{V}\right) = \boldsymbol{F}_{aero} + \boldsymbol{G} + \boldsymbol{P} \\ \dfrac{d\boldsymbol{H}}{dt} = \dfrac{\delta \boldsymbol{H}}{\delta t} + \boldsymbol{\omega} \times \boldsymbol{H} = \boldsymbol{M}_{aero} + \boldsymbol{M}_G + \boldsymbol{M}_P \end{cases} \tag{2}$$

where $m(t)$ is the instantaneous mass, $\boldsymbol{V}$ is flight velocity, $\boldsymbol{H}$ is momentum moment, $\boldsymbol{F}_{aero}$, $\boldsymbol{G}$ and $\boldsymbol{P}$ are respectively aerodynamic forces, gravity and thrust, while $\boldsymbol{M}_{aero}$, $\boldsymbol{M}_G$ and $\boldsymbol{M}_P$ are respectively moment from aerodynamic forces, gravity and thrust. $\boldsymbol{\Omega}$ and $\boldsymbol{\omega}$ are the rotational angular velocity of the rotational coordinate system relative to the static coordinate system.

4.2 Rigid body dynamics model

The translational kinetic equations of the fuselage and four wings can be respectively written as

$$\begin{cases} \boldsymbol{F}_{aero\_f} + \boldsymbol{F}_{1\_f} + \boldsymbol{F}_{2\_f} + \boldsymbol{G}_f + \boldsymbol{P} = m_f \dfrac{d\boldsymbol{V}_f}{dt} \\ \boldsymbol{F}_{f\_1} + \boldsymbol{F}_{3\_1} + \boldsymbol{G}_1 + \boldsymbol{F}_{aero\_1} = m_1 \dfrac{d\boldsymbol{V}_1}{dt} \\ \boldsymbol{F}_{f\_2} + \boldsymbol{F}_{4\_2} + \boldsymbol{G}_2 + \boldsymbol{F}_{aero\_2} = m_2 \dfrac{d\boldsymbol{V}_2}{dt} \\ \boldsymbol{F}_{1\_3} + \boldsymbol{G}_3 + \boldsymbol{F}_{aero\_3} = m_3 \dfrac{d\boldsymbol{V}_3}{dt} \\ \boldsymbol{F}_{2\_4} + \boldsymbol{G}_4 + \boldsymbol{F}_{aero\_4} = m_4 \dfrac{d\boldsymbol{V}_4}{dt} \end{cases} \tag{3}$$

where $\boldsymbol{F}_{aero\_f}$ is the aerodynamic forces acting on the fuselage, $\boldsymbol{F}_{1\_f}$ is the forces acting on the fuselage generated by the movement of the wing, and the rest parameters follow the same naming rules. Based on (1) and (3), it can be obtained that

$$\boldsymbol{F}_{aero} + \boldsymbol{G} + \boldsymbol{P} = m\frac{d\boldsymbol{V}_B}{dt} + \sum_{i=1}^{4} m_i \frac{d\boldsymbol{V}_{S_i}}{dt} \tag{4}$$

Comparing with (2), the second term of the right side of (4) is the additional forces generated by the movement of the wings. Furthermore, omitting the subscript *i*, then

$$\frac{d\boldsymbol{V}_S}{dt} = \frac{d^2\boldsymbol{S}}{dt^2} = \frac{d}{dt}\left(\frac{\delta \boldsymbol{S}}{\delta t} + \boldsymbol{\omega} \times \boldsymbol{S}\right) = \frac{\delta^2 \boldsymbol{S}}{\delta t^2} + 2\boldsymbol{\omega} \times \frac{\delta \boldsymbol{S}}{\delta t} + \frac{\delta \boldsymbol{\omega}}{\delta t} \times \boldsymbol{S} + \boldsymbol{\omega} \times (\boldsymbol{\omega} \times \boldsymbol{S}) \tag{5}$$

The rotational kinetic equations can be obtained through similar deductions. For the *i*th wing, according to the definition of Momentum moment, it can be written as

$$\boldsymbol{H}_i = \int \boldsymbol{S}_i^* \times \boldsymbol{V}_i^* dm_i^* = \int \boldsymbol{S}_i^* \times \left(\boldsymbol{V}_o + \frac{d\boldsymbol{S}_i^*}{dt}\right) dm_i^* \tag{6}$$

Through derivation,

$$\frac{d\boldsymbol{H}_i}{dt} = m_i \frac{d\boldsymbol{S}_i}{dt} \times \boldsymbol{V}_o + m_i \boldsymbol{S}_i \times \frac{d\boldsymbol{V}_o}{dt} + m_i \boldsymbol{S}_i \times \frac{d^2 \boldsymbol{S}_i}{dt^2} \quad \textbf{(7)}$$

Also,

$$\frac{d\boldsymbol{H}_i}{dt} = \int \boldsymbol{S}_i^* \times \frac{d\boldsymbol{V}_i^*}{dt} dm_i^* + \int \frac{d\boldsymbol{S}_i^*}{dt} \times \boldsymbol{V}_i^* dm_i^* = \boldsymbol{M}_{oi} + \int \frac{d\boldsymbol{S}_i^*}{dt} \times (\frac{d\boldsymbol{S}_i^*}{dt} + \boldsymbol{V}_o) dm_i^* = \boldsymbol{M}_{oi} + m_i \frac{d\boldsymbol{S}_i}{dt} \times \boldsymbol{V}_o \quad \textbf{(8)}$$

Comparing the above two equations (7) and (8), it can be obtained that

$$\boldsymbol{M}_{oi} = m_i \boldsymbol{S}_i \times \frac{d\boldsymbol{V}_o}{dt} + m_i \boldsymbol{S}_i \times \frac{d^2 \boldsymbol{S}_i}{dt^2} \quad \textbf{(9)}$$

where $\boldsymbol{M}_{oi}$ is the moment caused by the movement of the *i*th wing, then

$$\begin{cases} \boldsymbol{M}_{aero\_B} + \boldsymbol{M}_{1\_B} + \boldsymbol{M}_{2\_B} = \dfrac{d\boldsymbol{H}_B}{dt} \\ \boldsymbol{M}_{B\_1} + \boldsymbol{M}_{3\_1} + \boldsymbol{M}_{G_1} + \boldsymbol{M}_{aero\_1} = m_1 \boldsymbol{S}_1 \times \dfrac{d\boldsymbol{V}_o}{dt} + m_1 \boldsymbol{S}_1 \times \dfrac{d^2 \boldsymbol{S}_1}{dt^2} \\ \boldsymbol{M}_{B\_2} + \boldsymbol{M}_{4\_2} + \boldsymbol{M}_{G_2} + \boldsymbol{M}_{aero\_2} = m_2 \boldsymbol{S}_2 \times \dfrac{d\boldsymbol{V}_o}{dt} + m_2 \boldsymbol{S}_2 \times \dfrac{d^2 \boldsymbol{S}_2}{dt^2} \\ \boldsymbol{M}_{1\_3} + \boldsymbol{M}_{G_3} + \boldsymbol{M}_{aero\_3} = m_3 \boldsymbol{S}_3 \times \dfrac{d\boldsymbol{V}_o}{dt} + m_3 \boldsymbol{S}_3 \times \dfrac{d^2 \boldsymbol{S}_3}{dt^2} \\ \boldsymbol{M}_{2\_4} + \boldsymbol{M}_{G_4} + \boldsymbol{M}_{aero\_4} = m_4 \boldsymbol{S}_4 \times \dfrac{d\boldsymbol{V}_o}{dt} + m_4 \boldsymbol{S}_4 \times \dfrac{d^2 \boldsymbol{S}_4}{dt^2} \end{cases} \quad \textbf{(10)}$$

Furthermore , the vector equations (10) can be rewritten as

$$\boldsymbol{M}_{aero} + \sum_{i=1}^{4} \boldsymbol{M}_{G_i} - \sum_{i=1}^{4} m_i (\boldsymbol{S}_i \times \frac{d\boldsymbol{V}_o}{dt} + \boldsymbol{S}_i \times \frac{d^2 \boldsymbol{S}_i}{dt^2}) = \frac{d\boldsymbol{H}_B}{dt} \quad \textbf{(11)}$$

where,

$$\frac{d\boldsymbol{V}_o}{dt} = \frac{\delta \boldsymbol{V}_o}{\delta t} + \boldsymbol{\omega} \times \boldsymbol{V}_o \quad \textbf{(12)}$$

4.3 Simplified longitudinal dynamic model

The vector equations (4) and (11) are very complicated expressions when we try to get the component expressions. For example, (5) can be rewritten as vector form

$$\begin{bmatrix} \dot{V}_{x1} \\ \dot{V}_{y1} \\ \dot{V}_{z1} \end{bmatrix} = \begin{bmatrix} \ddot{s}_x \\ \ddot{s}_y \\ \ddot{s}_z \end{bmatrix} + 2 \cdot \begin{bmatrix} \dot{s}_z \omega_y - \dot{s}_y \omega_z \\ \dot{s}_x \omega_z - \dot{s}_z \omega_x \\ \dot{s}_y \omega_x - \dot{s}_x \omega_y \end{bmatrix} + \begin{bmatrix} s_z \dot{\omega}_y - s_y \dot{\omega}_z \\ s_x \dot{\omega}_z - s_z \dot{\omega}_x \\ s_y \dot{\omega}_x - s_x \dot{\omega}_y \end{bmatrix} + \begin{bmatrix} -s_x \omega_y^2 + s_y \omega_x \omega_y - s_x \omega_z^2 + s_z \omega_x \omega_z \\ -s_y \omega_x^2 + s_x \omega_y \omega_x - s_y \omega_z^2 + s_z \omega_y \omega_z \\ -s_z \omega_x^2 + s_x \omega_z \omega_x - s_z \omega_y^2 + s_y \omega_z \omega_y \end{bmatrix} \quad \textbf{(13)}$$

where $\omega_x, \omega_y, \omega_z$ and s_x, s_y, s_z are the projections of the vector $\boldsymbol{S}$ and $\boldsymbol{\omega}$ under the fuselage coordinate system.

Undoubtedly, (16) is not conducive to the calculation and it can usually be simplified as the longitudinal dynamic model.

Under asymmetric deformation conditions,

$$\boldsymbol{S}_i = \begin{bmatrix} -s_{ix} & 0 & s_{iz} \end{bmatrix}^T, \omega = \begin{bmatrix} 0 & 0 & \omega_z \end{bmatrix}^T, V = \begin{bmatrix} V_x & V_y & 0 \end{bmatrix}^T \quad \textbf{(14)}$$

where s_{ix} and s_{iz} can be obtained from geometric relationships shown in Fig.8

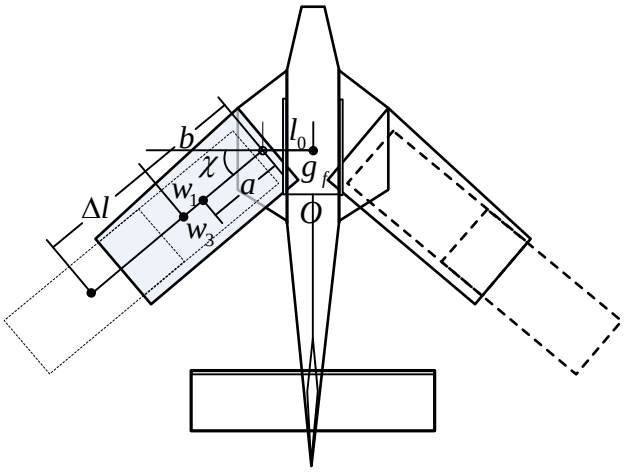

Figure 8: geometric relationships between variable wing.

For the lift variable-sweep wing and the lift variable-span wing,

$$\begin{cases} s_{1x} = a\sin\chi \\ s_{1z} = a\cos\chi + l_0 \end{cases} \quad \textbf{(15)}$$

$$\begin{cases} s_{3x} = (b+\Delta l)\sin\chi \\ s_{3x} = (b+\Delta l)\cos\chi + l_0 \end{cases} \quad \textbf{(16)}$$

The expression of the additional forces due to the *i*th wing can be obtained based (5), (13) and (14),

$$\begin{bmatrix} F_{ix} \\ F_{iy} \\ F_{iz} \end{bmatrix} = m_i \left(\begin{bmatrix} \ddot{s}_{ix} \\ 0 \\ \ddot{s}_{iz} \end{bmatrix} + 2 \cdot \begin{bmatrix} 0 \\ -\dot{s}_{ix}\omega_z \\ 0 \end{bmatrix} + \begin{bmatrix} 0 \\ -s_{ix}\dot{\omega}_z \\ 0 \end{bmatrix} + \begin{bmatrix} s_{ix}\omega_z^2 \\ 0 \\ 0 \end{bmatrix} \right) \quad \textbf{(17)}$$

The expression of the additional moments due to the *i*th wing can be obtained based (11), (12) and (14),

$$\begin{bmatrix} M_{ix} \\ M_{iy} \\ M_{iz} \end{bmatrix} = m_i \left(\begin{bmatrix} s_{iz}(2\dot{s}_{ix}\omega_z + s_{ix}\dot{\omega}_z) \\ s_{ix}\ddot{s}_z + s_{iz}(\ddot{s}_{ix} + s_{ix}\omega_z^2) \\ s_{ix}(2\dot{s}_{ix}\omega_z + s_{ix}\dot{\omega}_z) \end{bmatrix} + \begin{bmatrix} -s_{iz}(\dot{V}_y + V_x\omega_z) \\ s_{ix}\dot{V}_z + s_{iz}(\dot{V}_x - V_y\omega_z) \\ -s_{ix}(\dot{V}_y + V_x\omega_z) \end{bmatrix} \right) \quad \textbf{(18)}$$

3. Conclusion

The main characteristics of this UAV are as follows:

The larger-scale deformation characteristics provide the UAV a better adaptability for different flight velocity and airspace. Through a reasonable mission planning and control system design, the UAV is able to maintain optimal flight performance under the entire process of single flight task, and also variety of different tasks.
Considering the asymmetric deformation of the aerodynamic configuration, the UAV can obtain asymmetric aerodynamics distribution, and thus achieves attitude motion. The aerodynamic effects caused by the asymmetric variable-span wing can be used to replace that of the traditional aileron, being expected to provide considerable rolling moment. Accordingly, by the active asymmetric deformation, the UAV can obtain the desired attitude control.
The studies in this paper mainly focus on the following aspects:
Design the aerodynamic configuration of the UAV with variable-span wing and variable-sweep wing, analyze the structural properties and determine the reasonable range of deformation parameters. Calculate the aerodynamics through the Computational Fluid Dynamics method and engineering prediction method and analyze the aerodynamic characteristics of the typical static configurations which are shown in Fig.2.
Establish the multi-rigid-body model of the UAV. Designate the fuselage as the primary rigid body, then the variable-span wing and variable-sweep wing as the subsidiary rigid bodies. Define the appropriate generalized coordinates and generalized velocity according to the constraint relations between the primary rigid body and subsidiary rigid body, and then obtain the kinetic model of first-order differential equations.
The paper should not exceed 15 pages. Please upload your file in plain portable document format (pdf) only, i.e. the file should not be protected nor in any other format.The submitted pdf file should not exceed 10 Megabytes. If your file is much larger, there is probably a figures resolution problem. This should be fixed when creating the pdffile. The editorial team will take care of protecting the paper after verification of the layout.

References

[1] Armando R Rodriguez. Morphing Arictaft technology survey[R]. A IAA 2007-1258, 2007.
[2] Wei min S, Nian xu C. Development and Key Technologies of theMorphing Aircraft[J]. FLIGHT DYNAM ICS.2009.12: Vol27 No.6: 5-8.
[3] Janisa J. Henry，Darryll J. Pines. A Mathematical Model for Roll Dynamics by Use of a Morphing-Span Wing [J].AIAA.2007.4:23-26
[4] Onur Bilgen, Lauren M.ButtSteven R.Day. A Novel Unmanned Aircraft with Solid State Control Surfaces: Analysis and Flight Demonstration [J].AIAA.2011.4:4-7.
[5] Smith K，Butt J，Von Spakovsky M R. A Study of the Benefits of Using Morphing Wing Technology In Fighter Aircraft Systems[R]. AIAA2007-4616，2007.
[6] Namgoong H, Crossley W A, Lyrintzis A S. Aerodynamic optimization of a morphing airfoil using energy as an objective[J]. AIAA Journal, 2007, 45(9): 2113-2124.
[7] J. Mestrinho，P. Gamboa，P. Santos. Design Optimization of a Variable-Span Morphing Wing for a Small UAV [J].AIAA.2011.4:2-7.
[8] William A. Crossley, Michael D. Skillen, Joshua B. Frommer, Brian D. Roth. Morphing Aircraft Sizing Using Design Optimization [J]. AIAA. 2011. 3:612-621.
[9] [9]. Gamboa P, Vale J, Lau F J P, Suleman A. Optimization of a morphing wing based on coupled aerodynamic and structural constraints[J]. AIAA Journal,2009, 47(9): 2087-2103.
[10] Gandhi N，Jha A，Monaco J. Intelligent Control of a Morphing Aircraft[R]. AIAA 2007-1716，2007.
[11] B. Obradovic, K. Subbarao. Modeling of Dynamic Loading of Morphing-Wing Aircraft[J]. J OURNAL OF AIRCRAFT Vol. 48, No.2, March–April 2011.
[12] Guclu Seber, Evren Sakarya. Nonlinear Modeling and Aeroelastic Analysis of an Adaptive Camber Wing[J]. JOURNAL OF AIRCRAFT Vol.47, No.6, November–December 2010.
[13] Andersen G, Cowan D, Piatak D. Aeroelastic modeling,analysis and testing of a morphing wing structure[R].AIAA-2007-1734, 2007.
[14] David A. Perkins, John L. Reed, Jr., Ernie Havens. Morphing Wing Structures for Loitering Air Vehicles[J].AIAA.2004.4.19-1888.
[15] Edward A. Bubert, Benjamin K. S. Woods, Curt S. Kothera, Norman M. Wereley. Design and Fabrication of a Passive 1-D Morphing Aircraft Skin[J]. 49th AIAA/ ASME/ ASCE/AHS/ASC Structures, Structural Dynamics, and Materials Conference 16th 7-10 April 2008, Schaumburg, IL.
[16] Henry J, Blondeau J.,Pines D. Stability Analysis for UAVs with a Variable Aspect Ratio Wing. 46th AIAA/ASME/ASCE/AHS/ASC Structures, Structural Dynamics and Materials Conference, Austin, Texas, April 18-21, 2005.
[17] David A. Neal, Matthew G. Good, Christopher O. Johnston, elt. Design and Wind-Tunnel Analysis of a Fully Adaptive Aircraft Configuration[J].AIAA 2004-1727.

[18] Frank E. Fresconi, Ilmars Celmins. Obtaining the Aerodynamic and Flight Dynamic Characteristics of an Asymmetric Projectile Through Experimental Spark Range Firings[J].AIAA.2011.08.11-6334.
[19] B. Obradovic, K. Subbarao. Design and Simulation of a Morphing-wing Controller with Actuator Loading Penalization [J].AIAA.2011.8:08-11.Rini, P. 2006. Analysis of differential diffusion phenomena in high enthalpy flows, with application to thermal protection material testing in ICP facilities. PhD Thesis. Université Libre de Bruxelles, Faculté des Sciences Appliquées.